

Article ID 1004-924X(2007)12-1932-14

# 单通道和多通道毛细管光学元件—技术发展水平和应用

A Bjeoumikhov<sup>1</sup>, R Wedell<sup>2</sup>, S Bjeoumikhova<sup>3</sup>

(1. IfG Institute for Scientific Instruments GmbH, 12489 Berlin, RudowerChaussee 29/31, Germany;

2. Institut für angewandte Photonik e. V., 12489 Berlin, RudowerChaussee 29/31, Germany;

3. Bundesanstalt für Materialforschung und-prüfung, 12200 Berlin, Germany)

**摘要:**毛细管光学元件在 X 射线分析中的应用已有 20 多年的历史,在这段时间里,毛细管光学元件的制作技术发生了很大的变化。上世纪 90 年代初,使用的是组装的毛细管光学元件,目前,集成的多通道毛细管光学元件已广泛地应用于市场销售的 X 射线分析设备中。这些元件的毛细管直径在微米量级,其光学性质可以根据几何光学的光线追迹计算进行描述。最近,由于多通道毛细管制作技术的改进,已成功制成了 200 nm 及以下通道尺寸的毛细管光学元件。在这样小的通道尺寸下,观察到了 X 射线辐射的波动效应。最后文章介绍了毛细管光学元件在 X 射线微荧光分析和微衍射方面的应用。

**关键词:**X 射线毛细管光学元件;波动特性;纳米毛细管;X 射线分析

**中图分类号:**O434.19;O436.1 **文献标识码:**A

## Mono- and polycapillary optics-State of the art and applications

A Bjeoumikhov<sup>1</sup>, R Wedell<sup>2</sup>, S Bjeoumikhova<sup>3</sup>

(1. IfG Institute for Scientific Instruments GmbH, 12489 Berlin, RudowerChaussee 29/31, Germany;

2. Institut für angewandte Photonik e. V., 12489 Berlin, RudowerChaussee 29/31, Germany;

3. Bundesanstalt für Materialforschung und-prüfung, 12200 Berlin, Germany)

**Abstract:** For more than 20 years, capillary optics have been used in X-ray analytics. During this time the technology of manufacturing capillary optics passed a considerable development. Whereas in the beginning of 1990s assembled capillary optics were tested in research laboratories, at present monolithic polycapillary optics are widely used in commercial X-ray analytical instruments. These optics show capillary sizes in the micrometer region and their physical behaviour can be described in terms of geometrical optics using ray tracing programs. Recently capillary channel sizes of 200 nm and below were realised due to further improvement of the manufacturing technology for polycapillary structures. At such small structures, the appearance of wave effects for X-ray radiation was observed. Finally, application examples for capillary optics in micro X-ray fluorescence analysis and micro X-ray diffractometry are presented.

**Key words:** X-ray capillary optics; wave properties; nanocapillary; X-ray analytics

## 1 Introduction

The capillary optics is based on the effect of total external reflection which had been discovered by Compton<sup>[1]</sup> in 1923. Using this principle in a cylindrical capillary, X-ray radiation can be transported by means of multiple reflections. This method was already applied for X-ray radiation transport in the end of the twenty years of the last century<sup>[2]</sup>. The intensity of the radiation at a defined distance from the source is increased by such an optical element in comparison to a pinhole without capillary. If the capillary is slightly bent radiation will be still transported but the intensity losses are higher than in the case of a straight capillary. However, the transmission degree is acceptable for not too small radii of curvature. Using a bundle of many bent capillaries arranged in layers by several fixation grids with regular holes, a focusing optical system was realised by Kumakhov *et al.*<sup>[3-4]</sup>. At the entrance and the exit of the optical system, the capillaries are directed to a focal point. In the first systems, monocapillaries were used but later also polycapillaries were assembled as an X-ray lens. Such an X-ray lens was successfully

used to realise X-ray fluorescence analysis with spatial resolution<sup>[5]</sup>. A considerable improvement of the manufacturing technology was achieved by glass drawing technology for fabrication of monolithic capillary lenses (see *e. g.* [6]). At present this technology is used in all laboratories and companies where X-ray capillary optics are manufactured.

## 2 Experimental study of a focal spot intensity distribution of a polycapillary lens

In this paragraph the intensity distribution in focal spots of a polycapillary lens is studied experimentally. The main geometrical parameters are the capillary channel size  $d_c$ , the length  $L$ , the focal distances  $f_1$  at the entrance and  $f_2$  at the exit as well as the cross section size. Further parameters are  $D_{in}$ , the diameter of the lens at the entrance,  $D_{max}$ , the maximum diameter of the lens,  $D_{out}$ , the diameter of the lens at the exit and  $R = f_1 + L + f_2$ , the distance between source spot and focal spot. These parameters are given in Tab. 1.

Tab. 1 Geometrical parameters of the polycapillary lens

$f_1/\text{mm}$	$f_2/\text{mm}$	$L/\text{mm}$	$D_{in}/\text{mm}$	$D_{out}/\text{mm}$	$D_{max}/\text{mm}$	$R/\text{mm}$	$d_c/\mu\text{m}$
57.8	16.9	80.8	4.8	4.1	7.2	155.5	9.5

The capillary channel sizes presented in Tab. 1 correspond to the central part of the lens where they have maximum values.

The experimental determination of focal spot size was carried out according to a method described in [7]. A microfocus X-ray tube with an anode spot of  $50 \mu\text{m}$  was used as source. The employed silicon drift detector has an active area of  $4 \text{ mm}^2$ . For the measurement of the intensity distribution at the entrance window, a pinhole

diaphragm of  $10 \mu\text{m}$  in diameter was positioned. The measured focus spot sizes in the energy interval  $3 \sim 25 \text{ keV}$  lie between  $20 \mu\text{m}$  and  $30 \mu\text{m}$  as determined at the half maximum of the intensity (FWHM).

Usually, the size of the focal spot of a polycapillary lens is estimated by the formula  $\Delta X_{ph} \approx \theta_c f_2$  where  $\theta_c$  is the critical angle and  $f_2$  is the focal distance at the lens exit. For example, the above mentioned formula gives with  $\theta_c = 4 \text{ mrad}$

for 8 keV a focal spot size of about  $60 \mu\text{m}$ .

The reason for such large deviations between calculated and measured values and the values for different lenses can be clarified by a careful measurement of two-dimensional radiation intensity distributions in the focal plane. Such a measurement was carried out by a two-dimensional scan with a detector equipped with a pinhole diaphragm. Fig.1 shows the obtained results for the energies 3~5 keV, 10~15 keV,

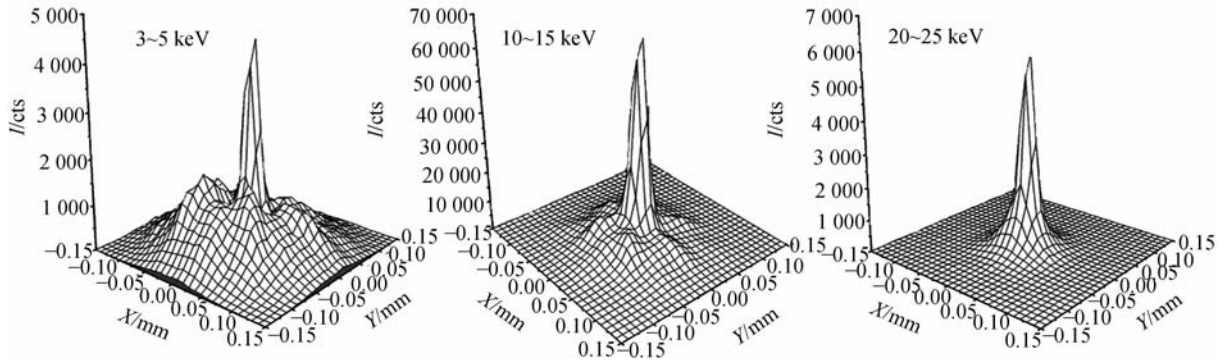


Fig. 1 Measured two-dimensional intensity distributions in the focus of the polycapillary lens with the parameters given in Tab. 1

The possibility of appearance of such a fine structure in the focus of a polycapillary lens has been shown already in model calculations (see [8]). The reason for this effect is the hexagonal packaging of the structure and the hexagonal form of capillaries in their cross section. The fine structure observed in the early experiments during focussing synchrotron radiation by a half lens<sup>[9]</sup> can be also explained in terms of pure geometrical effects, in contrast to the explanations based on wave-optics effects<sup>[10]</sup>.

As a proof of the “geometrical” origin of the fine structure in Fig. 2, normalized linear radiation intensity distributions are shown corresponding to different energy intervals. As seen from this diagram the positions of the maxima corresponding to satellite lines do not depend on energy. The distance from the central peak to the centre of satellite peaks amounts  $0.065 \text{ mm}$  for all energy intervals. If the origin of satellite lines will be their “wave” character then due to

and  $25 \sim 30 \text{ keV}$ . In all energy intervals in the distribution centre a sharp narrow peak is observed surrounded by exact 6 satellite peaks. The intensity of satellite peaks decreases with increasing energy and they disappear totally in the energy interval  $20 \sim 25 \text{ keV}$ . If the focal spot size is determined by FWHM then this value corresponds only to the width of the central peak and does not take into account the specific intensity distribution outside this peak.

the dispersion the positions of these maxima should depend on energy (wavelength). Furthermore, with increasing radiation energy the satellites disappear. This seems to be due to the smallness of the corresponding values of critical angles. The angular position of satellites corresponds to the value  $\Delta X/f_2 = 0.065/16.9 = 3.9 \text{ mrad}$ .

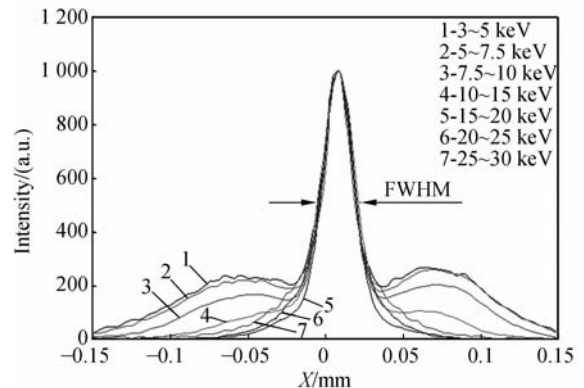


Fig. 2 Linear radiation intensity distribution in the focus of the polycapillary lens

Why will a fine structure not be observed in all cases? The following factors are important for the appearance of this effect: a high precision in manufacturing of the entire lens shape, smoothness of the capillary channel trajectories, maintenance of long-distance order for packaging and orientation of capillary channels, minimum sizes of the source and high precision of adjustment of the lens relative to the source. All these conditions must be guaranteed simultaneously.

### 3 X-ray propagation through a 200 nm capillary structure

A polycapillary structure with channel sizes of 200 nm has been manufactured. The outside diameter of the entire structure amounts 300  $\mu\text{m}$ . Fig. 3 shows an electron microscope image of a part of this structure. As seen, the channels are circular, regularly arranged and of equal size.

For investigation of the properties of the

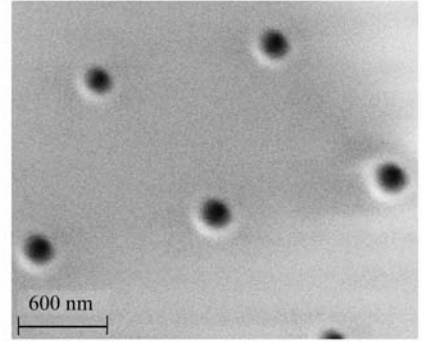


Fig. 3 Image of the polycapillary structure taken at scanning electron microscope

given structure an X-ray experimental arrangement was built up as shown in Fig. 4. A shift of the source and the detector perpendicular to the axis of capillary channels must be realised (see Fig. 4(a)). In this experiment for detecting X-ray radiation, not only a CCD camera but also an energy dispersive SDD are used. At the entrance window of the SDD a 10  $\mu\text{m}$  pinhole diaphragm was mounted. The source and the detector are positioned symmetrically relative to the structure at a distance of 480 mm each.

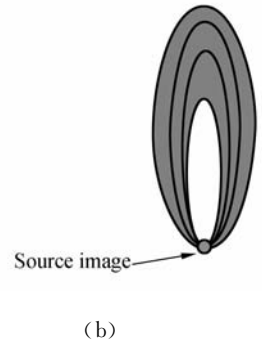
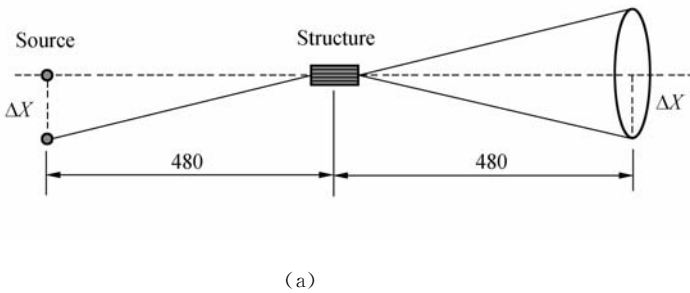


Fig. 4 (a) Scheme of measurement of the polycapillary structure (b) Image of radiation scattering at a shift of the source from the central axis of the structure

In the case of a single capillary of circular shape the axis of which is shifted by  $\Delta X$  relative to the position of the source, behind the capillary in the focal plane a ring-shaped radiation distribution with a diameter of  $2 \Delta X$  is observed. The width of the ring is determined by the size of the source and the capillary diameter. In the case of a polycapillary structure the outside diameter of

the structure influences the distribution pattern. Here an image is observed which is shown schematically in Fig. 4(b). This image is a superposition of rings with different diameters but having a common point at their periphery determined by the source position.

Fig. 5 shows an image taken in the focal plane if the source is shifted by 300  $\mu\text{m}$  relative

to the structure axis. As source a microfocus X-ray tube with Mo-anode and an anode spot size of  $50\ \mu\text{m}$  was used. This tube was operated at 40 kV and  $700\ \mu\text{A}$ . For studying the peculiarities of the intensity distribution at different radiation energies a scan with the SDD equipped with a  $50\ \mu\text{m}$  pinhole diaphragm at the entrance window was carried out along the line marked in Fig. 5. The obtained curves are presented in Fig. 6.

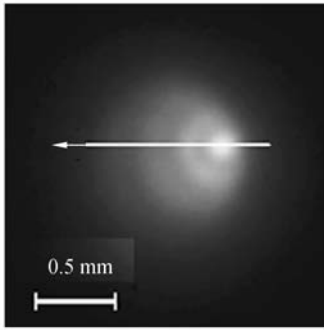


Fig. 5 Observable X-ray image in the focal plane of the polycapillary structure (circular capillary channels with a diameter of  $200\ \text{nm}$ ) at a shift of the source by  $300\ \mu\text{m}$

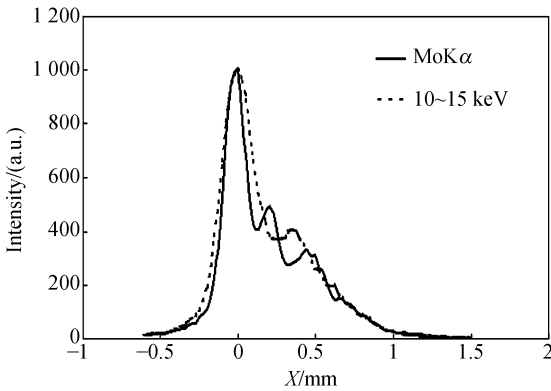


Fig. 6 Radiation intensity distribution of different radiation energies along the line marked in Fig. 5

As seen from the diagrams the distributions change their character in dependence on radiation energy. For the Mo- $K\alpha$  line ( $\lambda = 0.0708\ \text{nm}$ ), the distance between the first peak and the main zeroth peak amounts  $0.213\ \text{mm}$  whereas in the energy interval  $10\sim 15\ \text{keV}$  (mean wavelength  $\lambda = 0.0991\ \text{nm}$ ) this value amounts  $0.35\ \text{mm}$ .

The calculation of corresponding scattering angles  $\theta$  results in  $0.444\ \text{mrad}$  and  $0.729\ \text{mrad}$ , respectively. A re-calculation of the capillary channel diameter according to the formula  $d = (1.22)\lambda/\theta$  under consideration of mean radiation wavelengths gives for the first interval  $d = 195.2\ \text{nm}$  and for the second one  $d = 164.7\ \text{nm}$ . As mentioned above the real capillary channel diameter is approximately  $200\ \text{nm}$ . However, for a qualitative analysis the obtained results are satisfying. Obviously, the observed dependence of the intensity distribution at the exit of  $200\ \text{nm}$  capillary channels results from the wave properties of X-ray radiation. More details of these studies are published in [11].

## 4 Application of capillary optics in XRF and XRD

In this paragraph several examples are given for application of monocapillary optics and polycapillary lenses in X-ray analytics. The used lenses have channel diameters between  $1$  and  $100\ \mu\text{m}$ . The main application fields are X-ray fluorescence analysis and X-ray diffractometry. In the following subsections both fields are discussed in more detail.

### 4.1 X-ray fluorescence analysis with lateral resolution

#### 4.1.1 Measurement of the elemental distribution at the sample surface

In the conventional XRF the primary radiation irradiates a relative large surface area. An attempt to form a small sized spot by using a pinhole collimator leads to a catastrophic intensity loss. This means that the measurement time for one point will be already very long and the record of a two dimensional element distribution seems to be impossible. A high concentration of intensity within a small sized focal spot of the lens allows to realize elemental analysis with a high spatial resolution and a short measurement

time. Furthermore, it becomes possible to measure the two dimensional element distribution within a reasonable time. The implementation of micro-XRF using mono- and polycapillary optics combined with laboratory and synchrotron X-ray sources is described and discussed in many publications<sup>[12-17]</sup>. At synchrotron sources, focal spot sizes of about one micrometer can be achieved using shaped moncapillaries. Using for a two-step focusing a combination of an ellipsoidal moncapillary with a Fresnel zone plate, a focal spot size of 250 nm and a gain of more than 1 000 could be produced<sup>[18]</sup>. Here a 15 keV energy X-ray beam was focused in the first step Fresnel zone plate as a secondary source of 2.2  $\mu\text{m}$  vertically and 5  $\mu\text{m}$  horizontally in size. The ellipsoidal moncapillary makes a last final compression of the beam.

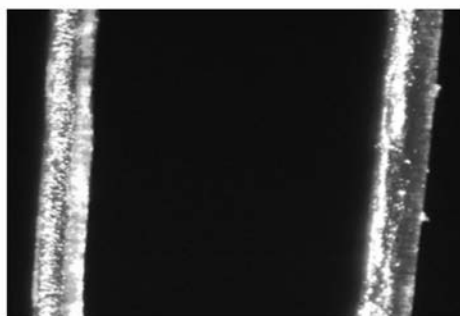
Modern polycapillary optics allow to focus X-ray beams to focal spot sizes of 15  $\mu\text{m}$ .

Micro XRF based on capillary optics can be also used for the determination of the elemental composition of samples having a small volume of a strong inhomogeneous element distribution. In the following example the elemental composition of human hairs was analyzed. For these measurements the XFlash detector manufactured by Bruker axs Microanalysis GmbH was used. Fur-

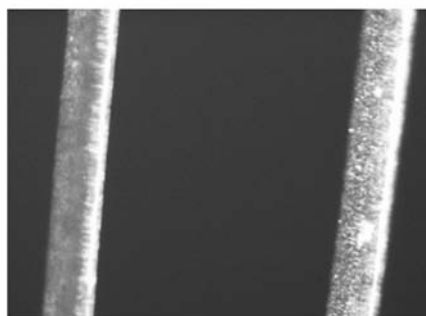
ther details of the measurement and other examples for micro XRF are given in [7].

Fig. 7 shows microscopic photographs of two hair types: dark and fair. The diameters of the hairs are 95  $\mu\text{m}$  (dark) and 80  $\mu\text{m}$  (fair), respectively. For every hair type two points were analyzed: near to the bottom and near to the end of a hair. For the dark hair the analyzed points are at 1 cm and 10 cm from the bottom and for the fair one at 2 cm and 5 cm, respectively. As well known the elemental composition of these parts of the same hair is different. A hair has a fiber structure and is therefore a material which strongly scatters X-radiation. For a considerable decrease of the scattered bremsstrahlung background, a filter made of Zr with a thickness of 75  $\mu\text{m}$  was used. The X-ray tube was operated at 40 kV and 700  $\mu\text{A}$ . The measurement time for every spectrum was 1 000 s.

Measured spectra from hair are shown in Fig. 8. Both types contain mainly the elements S, Ca, Fe, Cu, Zn, and Pb. In dark hairs Sr is present whereas in fair hairs this element was not observed. In both hair types the concentration of sulphur is higher near to the bottom than to the end, but for the elements Ca, Cu and Sr the concentration is higher at the end of hair.



(a)

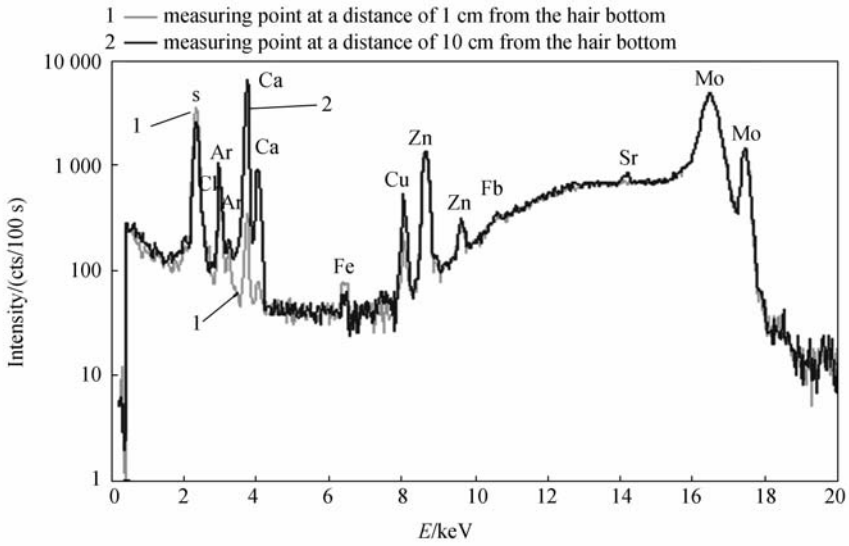


(b)

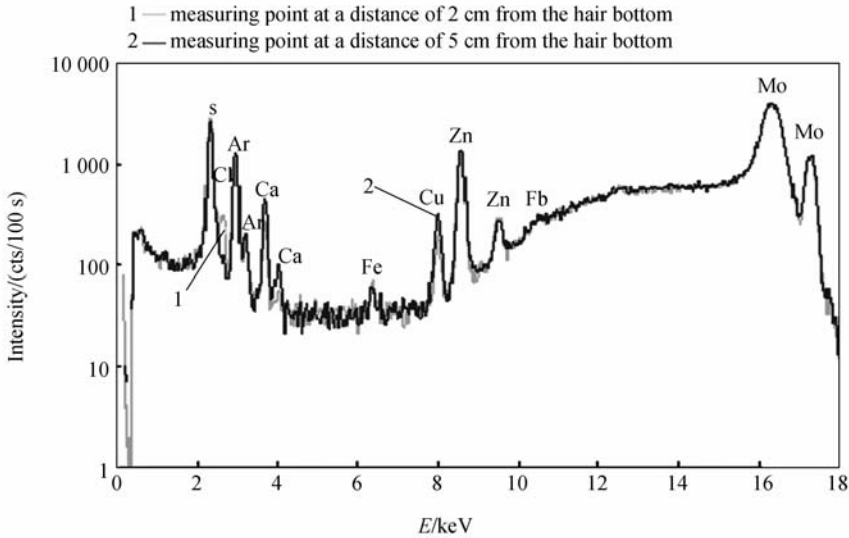
Fig. 7 Microphotograph of two hair types: (a) dark, (b) fair

Therefore, by using micro XRF it is possible to measure element distributions along hairs with high spatial resolution. This gives informa-

tion about the growing process of hairs and possible changes in the elemental composition due to different factors. Results of such analysis can be



(a)



(b)

Fig. 8 Spectra of two hair types: (a) dark, (b) fair

used for estimates of the environmental influence on the human health, of the affect of different shampoos, hair-dyes on the condition of hair etc.

#### 4.1.2 Measurement of the depth profile of an elemental distribution

Recently, the so-called 3D micro XRF analysis was realised on the basis of a selective registration of secondary fluorescence radiation emitted from different depth areas of the sample. For this purpose, in front of the detector, a so-called polycapillary conic collimator (Poly-CCC)<sup>[19-21]</sup>

or a polycapillary half-lens<sup>[22]</sup> are positioned. In this way an additional spatial resolution of micro XRF analysis into the sample depth is achieved within the limits of the exit depth of secondary radiation. These methods are realised by using a synchrotron source, because a rather high intensity is required. But recently it was shown that besides the use of powerful synchrotron sources also a combination of a microfocus X-ray tube with an efficient polycapillary lens provides enough intensity for the realisation of a tabletop 3D micro-XRF set-up<sup>[23-24]</sup> under laboratory condi-

tions. However, the sensitivity of the laboratory arrangement has to be taken one to two orders of magnitude lower than the synchrotron based set-up.

In [25] a new method for realisation of depth sensitive micro XRF analysis is proposed, which uses another method of registration of the secondary radiation than in the above mentioned publications<sup>[21-24]</sup>. For measurement of element distribution over the sample depth the well-known method of “knife-edge” is used. A simple element, a sharp edge of strong absorbing material is situated between sample and detector. Additionally, a slit in front of the detector is used to measure the intensity distribution over the depth. The principle of experimental arrangement is shown in Fig. 9.

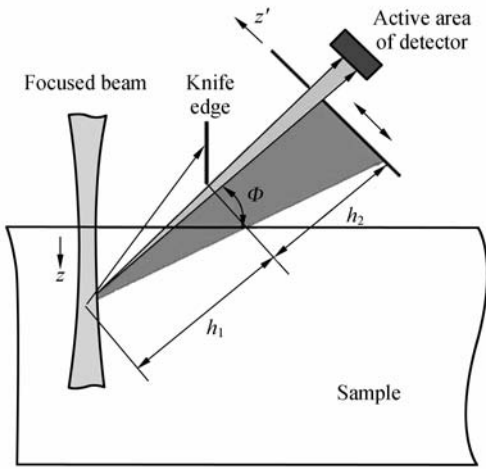


Fig. 9 Scheme of the principle of elemental depth distribution measurement by using the “knife-edge” method

Using geometrical relations as given in Fig. 9 and taking into account the absorption of the primary radiation and of the secondary fluorescence radiation by the corresponding absorption coefficients  $k_p$  and  $k_s$ , respectively, one finds for the elemental depth distribution:

$$n(Z) = C^{-1} I_p^{-1} j((h_2 / (h_1 \cos\Phi)) Z) \exp(k_s Z / \sin\Phi + k_p Z / \cos\Phi) . \quad (1)$$

This formula is correct for a homogeneous

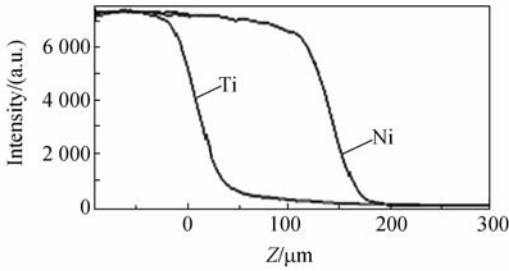
matrix consisting of a main element and a few other elements in a very low concentration so that they practically do not influence the absorption coefficients. Only under these conditions  $k_p$  and  $k_s$  may be assumed to be constant. For further details see [25].

For measurement of elemental depth distributions an experimental arrangement similar to the principle scheme shown in Fig. 9 was used. But here the angle of incidence for the primary beam and the registration angle for the secondary radiation are equal and have a value of  $45^\circ$ . A microfocus X-ray tube with an anode spot size of  $50 \mu\text{m}$  (anode material Mo) and a maximum power of 30 W has been used to generate the primary radiation. The beam focusing down to focal spot sizes between  $56 \mu\text{m}$  and  $29 \mu\text{m}$  was realised by a polycapillary lens. The knife edge is situated at a distance of  $h_1 = 8 \text{ mm}$  from the incident beam axis at the sample surface and the detector at a distance of  $h_1 + h_2 = 50 \text{ mm}$ . The detector slit width was  $50 \mu\text{m}$ . The factor  $h_2 / h_1$  of asymmetry “sample-knife-edge-detector” amounts 5.25. This means that the spatial depth resolution along the primary beam axis amounts  $\Delta Y = 50 \mu\text{m} / 5.25 = 9.5 \mu\text{m}$  and the coefficient for the scale transformation is given by  $Z = Z' \cos 45^\circ / 5.25 = 0.1347 Z'$ .

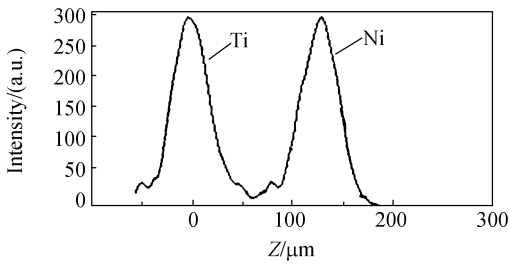
For a test of this method a sample consisting of two different metal layers ( $10 \mu\text{m}$  Ti and  $15 \mu\text{m}$  Ni) was used. The metal layers were fixed on foils with a thickness of  $100 \mu\text{m}$  adhesive on both sides. Fig. 10 shows this layered sample and the results of measurements. Clearly separated peaks from different materials are observed. The measured positions of the metallic layers corresponds to the real positions within a FWHM of about  $30 \mu\text{m}$ .

Besides the experimental determination of elemental depth distributions the knife-edge

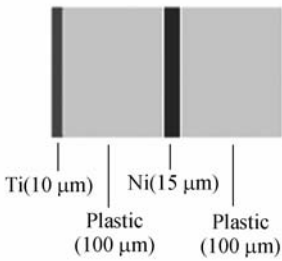
method can also be used to measure the surface profile of homogeneous strong absorbing samples. Details of this method are given in [25].



(a)



(b)



(c)

Fig. 10 (a) Measured distributions of fluorescence radiation intensities from a Ti-Ni layer structure (b) corresponding differentiated curves (c) scheme of the Ti-Ni layer structure

## 4.2 X-Ray diffractometry

### 4.2.1 X-ray structure analysis (single crystal diffractometry)

In the conventional X-ray structure analysis pinholes are used for collimation of the divergent primary X-ray beam. In this way the primary X-ray beam is directed on a sample consisting of an isolated single crystal of small dimensions (typically  $100 \sim 500 \mu\text{m}$ ) with a good parallelity.

However, in this case only a very small amount of the emitted radiation intensity can be used so that the measurement time becomes very long. The simplest way to increase the efficiency of the source is to substitute the pinhole collimator by a cylindrical capillary. Depending on the actual geometry such so-called X-ray guides will increase the radiation intensity at the crystal by several times due to the total reflection inside the capillary. Such an intensity increase results in a corresponding decrease of data collection time. Therefore, these optical elements are applied in many modern diffractometers for quite different purposes<sup>[26]</sup>.

### 4.2.2 Micro diffractometry

A further increase of the irradiation intensity at local analysis can be achieved by using a capillary of ellipsoidal form instead of a cylindrical one. Such an optical element realizes not only the radiation transport but also its concentration, so that a higher intensity gain can be reached. For example, in [27] stress analysis with a spatial resolution of  $70 \mu\text{m}$  has been performed.

For local diffractometric analyses also polycapillary lenses can be used. Fig. 11 schematically shows the realisation of an energy dispersive micro X-ray diffractometer.

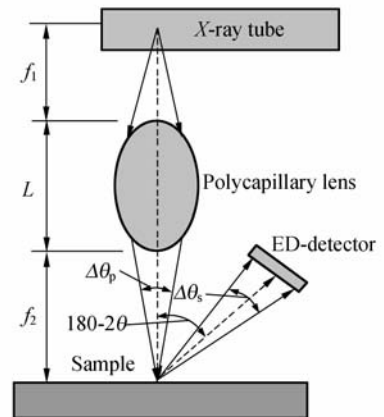


Fig. 11 Principle scheme of an energy dispersive micro X-ray diffractometer

A polycapillary lens is used to focus the divergent X-ray radiation emitted by a microfocus X-ray source on the sample surface. The anode material was molybdenum. The secondary radiation was detected by a Peltier cooled silicon drift detector with a 140 eV resolution at an energy of 6.4 keV. The measurements were carried out on a molybdenum sheet with a thickness of 50  $\mu\text{m}$ . The sample is mounted on a X-Y-table which is moved within 4 mm  $\times$  4 mm limits with steps of 0.05 mm and a dwell time of 3 s. Here, phase and texture in a selected small surface area can be estimated by the position and the intensity relations of the Laue diffraction peaks. By the described scanning, the sample surface changes in the texture can be measured. The resulting two-dimensional distributions of intensities of the Laue diffraction peaks (420) and (521) are shown in Fig. 12. It was observed that an intensity decrease of the (420) line corresponds to an intensity increase of the (521) line. More details are given in [28].

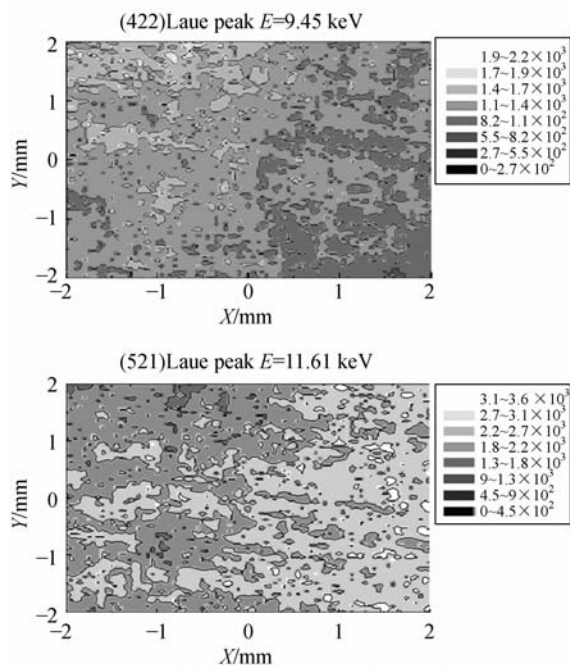


Fig. 12 Two-dimensional distributions of Laue diffraction peaks (420) and (521), respectively, across the surface of a Mo sample

#### 4.2.3 Analysis of polycrystals and powders

For powder diffractometry polycapillary semilenses can be used to convert the divergent primary X-ray radiation emitted from a microfocus tube into a quasiparallel beam. This beam is directed on the massive sample. Using a Soller slit or a plane secondary monochromator, the diffracted secondary radiation beam will be separated<sup>[29]</sup>. The use of such a collimating optics leads to a considerable increase of the diffracted intensity and therefore an corresponding decrease of the measurement time.

Using a focusing polycapillary lens, phase analysis can be carried out. In this case a relative large second focal distance is used. The sample in form of a foil or a powder hold between two X-ray transparent foils is positioned directly at the exit of the lens. The diffractogram is registered in the focal plane of the lens. For this purpose a single channel detector with a Two Theta Scan<sup>[30]</sup> or a bent position sensitive detector can be used. In these methods high intensities are achieved due to the relative large aperture of the polycapillary lenses.

At a synchrotron beam line a method of measurement has been realized, where the probe volume was imaged by detecting the small angle scattering of the primary synchrotron beam<sup>[31]</sup>. To separate the primary beam and the diffraction part, a parallel polycapillary structure was positioned between the sample and a CCD detector.

#### 4.3 Combination of X-ray methods with other analytical procedures

In the modern research and technology, different analytical methods of material characterisation are required. The combination of analytical procedures in one instrument allows the collection of the data of interest simultaneously and within a relative short time. In the following some examples of such instruments are shortly described.

In modern scanning electron microscopes, such a combination of of different analytical

methods can be realized. Their direct purpose is to obtain information about the surface morphology of samples with high resolution. The use of an additional module, *e. g.* an energy dispersive X-ray detector gives the opportunity to perform micro analysis to determine the element distribution in the sample, *i. e.* the realisation of electron probe micro analysis (EPMA). In [32] the development of a special X-ray source with a focusing polycapillary lens (iMOXS) for the application of micro-XRF in scanning electron microscopes (SEM) has been described. As well known, the sensitivity of microanalysis excited by an electron beam is lower than that by an X-ray beam due to excitation of a bremsstrahlung background by the charged electrons. Therefore, a combination of the high spatial resolution of a SEM image of the surface morphology with the high elemental detection sensitivity of micro-XRF is of great interest. Using such a special X-ray source, another analytical tool - X-ray diffractometry - can be also realised inside the SEM.

Fig. 13 shows the X-ray optical scheme of the realised diffractometer. The primary radiation is focused by a polycapillary lens on the sample surface where a focal spot of high intensity is realised. The diffracted radiation is registered by an energy dispersive detector in a scan-

ning procedure using a miniature goniometer. At the exit of the polycapillary lens a slit was positioned to collimate the primary beam and to guarantee a good angular resolution. The width of this slit can be regulated continuously. Also at the detector entrance an exchangeable slit is positioned. Therefore, the lens with the slit forms a fan-shaped beam in a quasi-one-dimensional focusing procedure which falls on the sample surface. Here a small sized line focal spot is formed. The diffractometry in a reflection geometry allows the realisation of a compact XRD module which can be mounted in a SEM.

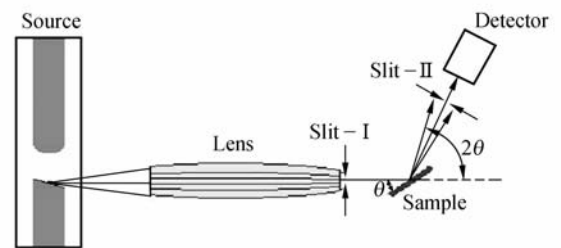


Fig. 13 X-ray optical scheme of the XRD module for SEM

After optimisation of the slit widths, diffractometric measurements were carried out using this experimental arrangement. An iMOXS source with a copper anode was used. Fig. 14 shows a diffractogram from a polycrystalline tungsten sample. The sample was fixed at an an-

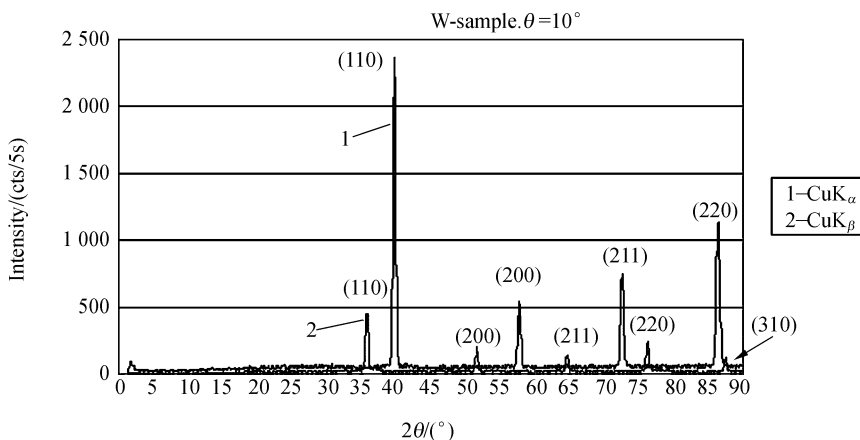


Fig. 14 Diffractogram of a polycrystalline tungsten sample

gle  $\Theta=10^\circ$ . In the diagram the reflexes obtained from the Cu-K $\alpha$  line and the Cu-K $\beta$  lines are shown. This became only possible due the energy resolution of the detector. Therefore, it was not necessary to use a K $\beta$  filter which would absorb more than 50 percent of the Cu-K $\alpha$  line. In this case the intensity of the main reflex (110) has a value of 460 cps.

First experimental results were presented at the Third German National Conference "Prozessnahe Röntgenanalytik" (X-Ray Analytics in Technological Processes) in November 2005<sup>[33]</sup>.

A further interesting solution is the combination of micro-XRF and Raman spectrometry within one instrument. Here the micro-XRF gives information about the elemental composition and the Raman spectrometer delivers data about the molecular structure of the sample.

The lateral resolution for micro-XRF amounts about 25  $\mu\text{m}$  and for Raman spectrometry about 5  $\mu\text{m}$ . The simultaneous analysis with both methods to determine the distribution of elements and molecules can be carried out in points or by scanning the sample surface. Such an instrument has been developed within the framework of the European project PRAXIS<sup>[34]</sup>.

## 5 Concluding remarks

The properties of capillary optics are mainly determined by the quality of manufacturing technology. A fine structure of the intensity distri-

bution in focal spots of polycapillary lenses will be only observed if a high precision in manufacturing of the entire lens shape is guaranteed, the long-distance order for packaging and orientation of capillary channels is maintained and the inner capillary channel walls show a high degree of smoothness. Further requirements concern the adjustment and the X-ray source spot size. The appearance of such a fine structure in the case of capillary channel sizes above 1  $\mu\text{m}$  can be explained by geometrical optics. In capillary structures with channels of 200 nm, the appearance of wave properties for X-ray radiation was observed.

At present, monolithic polycapillary optics with capillary channels of about 20 ~ 30  $\mu\text{m}$  are widely used in commercial X-ray analytical instruments. An efficient beam focusing enables the realisation of micro-XRF and micro-XRD where the intensity of the secondary radiation is high enough not only for a scan across the sample surface but also for a measurement of depth profiles.

The combination of micro-XRF and micro-XRD with other analytical methods offers new possibilities to characterize different samples. Especially, if micro-XRF and micro-XRD modules are adapted to scanning electron microscopes at these basic analytical instruments, useful additional methods of material research and testing will be available.

## References:

- [1] COMPTON A H. The total reflection of X-rays[J]. *Phil. Mag.*, 1923, 45: 1121.
- [2] JENTZSCH F. Optische Versuche mit Röntgenstrahlen (Optical Experiments with X-Rays) [J]. *Phys. Zeitschrift*, 1929, 30: 268-273.
- [3] KUMAKHOV M A. *Radiation of Channeled Particles in Crystals* [M]. Moscow: Ergoatomizdat, 1986.
- [4] ARKADEV V A, KOLOMIITSEV A I, KUMAKHOV M A, *et al.*. Wide-band X-ray optics with a large angular aperture[J]. *Sov. Phys. Usp.*, 1989, 32: 271-276.
- [5] YANG Y M, DING X L. An investigation of X-ray fluorescence analysis with an X-ray focusing system (X-ray lens) [J]. *Nucl. Instr. and Meth. in Phys. Res. B*, 1993, 82: 121-124.
- [6] GAO N, JANSSENS. *Polycapillary X-Ray Optics, in X-Ray Spectrometry: Recent Rechnological Advances* [M]. John Wiley & Sons Ltd, 2004.

- [7] BJEUMIKHOV A, LANGHOFF N, BJEUMIKHOVA S, *et al.*. Capillary optics for micro X-ray fluorescence analysis[J]. *Rev. Sci. Instrum.*, 2005, 76:063115-063115-7.
- [8] ARKADIEV V A, BZHAUMIKHOV A A, X-ray focusing in capillary structures[J]. *SPIE*, 1996, 2859:131-139.
- [9] DABAGOV S B, KUMAKHOV M A, NIKITINA S V. On the interference of X-rays in multiple reflection optics [J]. *Phys. Lett. A*, 1995, 203:279-282.
- [10] DABAGOV S B. Channeling of neutral particles in micro- and nanocapillaries[J]. *Physics Uspekhi*, 2003, 46:1053-1076.
- [11] BJEUMIKHOV A. Observation of peculiarities in angular distributions of X-ray radiation after propagation through polycapillary structures[J]. *Phys. Lett. A*, 2007, 360:405-410.
- [12] RINDBY A. Application of fiber technique in the X-ray region[J]. *Nucl. Instr. and Methods in Phys. Res. Sect. A*, 1986, 249:536-540.
- [13] DING X L, HE Y H, YAN Y M. Monolithic X-ray focusing lens for XRF analysis[J]. *Journal of Beijing Normal University (Natural Science)*, 1995, 31:75-79.
- [14] GAO N, PONOMAREV I Y, XIAO Q F, *et al.*. Enhancement of microbeam X-ray fluorescence analysis using monolithic polycapillary focusing optics[J]. *Appl. Phys. Lett.*, 1997, 71:3441-3443.
- [15] BRONK H, RÖHRS S, BJEUMIKHOV A, *et al.*. ArtTAX-a new mobile spectrometer for energy-dispersive micro X-ray fluorescence spectrometry on archeological objects[J]. *Fresenius J. Anal. Chemistry*, 2001, 371:307-316.
- [16] BJEUMIKHOV A, LANGHOFF N, WEDELL R, *et al.*. New generation of polycapillary lenses; manufacture and applications[J]. *X-Ray Spectrometry*, 2003, 32:172-178.
- [17] MACDONALD C A, GIBSON W M. Applications and advances in polycapillary optics[J]. *X-Ray Spectrometry*, 2003, 32:258-268.
- [18] SNIGIREV A, BJEUMIKHOV A, ERKO A, *et al.*. Submicrometer hard X-ray focusing using a single-bounce ellipsoidal capillary combined with a Fresnel zone plate[J]. *Journal of Synchrotron Radiation*, 2007, 14:227-228.
- [19] BZHAUMIKHOV A A, LANGHOFF N, SCHMALZ J, *et al.*. Polycapillary conic collimator for micro-XRF[J]. *SPIE*, 1998, 3444:430-435.
- [20] FIORINI C, LONGONI A, BJEUMIKHOV A, *et al.*. A new detection system with polycapillary conic collimator for high-localized analysis of X-ray fluorescence Emission[J]. *IEEE Trans. on Nucl. Sci.*, 2001, 48:268-271.
- [21] KANNIGEBER B, MALZER W, REICHE I. A new 3D micro X-ray fluorescence analysis set-up-first archeometric applications[J]. *Nucl. Instr. and Methods in Phys. Res. B*, 2003, 211:259-264.
- [22] VINCZE L, VEKEMANS B, BRENKER F, *et al.*. Three-dimensional trace element analysis by confocal X-ray microfluorescence imaging[J]. *Analytical Chemistry*, 2004, 76:6786-6791.
- [23] KANNIGEBER B, MALZER W, RODRIGUEZ A F, *et al.*. 3D micro-XRF investigations of paint layers with a table top set-up[J]. *Spectr. Chim. Acta B*, 2005, 60:41-47.
- [24] MALZER W. 3D Mikro-Röntgenfluoreszenzanalyse (3D micro X-ray fluorescence analysis) [D]. *Universität Bremen*, 2004.
- [25] BJEUMIKHOV A, BJEUMIKHOVA S, WEDELL R, *et al.*. A new method of depth sensitive micro X-ray fluorescence analysis[J]. *Nucl. Instr. and Methods in Phys. Res. B*, 2006, 248:142-149.
- [26] WEDELL R. Röntgenlichtleiter in der Analysetechnik (X-ray guides in analytics) [J]. *Phys. Blätter*, 1996, 52 (11):1134-1136.
- [27] EIGENMANN B, LANGHOFF N, BJEUMIKHOV A, *et al.*. Advantageous use of glass capillaries as primary optics for X-ray residual stress analyses and a novel concept for 'Micro diffraction stress analysis' [J]. *Materials Science Forum*, 2002, 404-407:303-308.
- [28] BJEUMIKHOV A, BJEUMIKHOVA S, LANGHOFF N, *et al.*. Polycapillary optics for energy dispersive micro X-ray diffractometry [J]. *Appl. Phys. Lett.*, 2005, 86:144102-1-144102-3.
- [29] GUBAREV M, CISZAK E, PONOMAREV I, *et al.*. First result from a macromolecular crystallography system with a polycapillary collimating optic and a microfocus X-ray generator [J]. *J. Appl. Crystallogr.*, 2000, 33:882-887.

- [30] BJEOUNIKHOV A, LANGHOFF N, RABE J, *et al.*. A modular system consisting of a microfocus X-ray source and different capillary optics for XRF and XRD applications[J]. *X-ray Spectrometry*, 2004, 33:312-316.
- [31] WROBLEWSKI T, BJEOUNIKHOV A. Small-angle X-ray imaging[J]. *Nucl. Instr. and Methods in Phys. Res. A*, 2004, 521:571-575.
- [32] BJEOUNIKHOV A, ARKADIEV V, EGGERT F, *et al.*. A new microfocus X-ray source, iMOXS, for high sensitive XRF analysis in scanning electron microscopes[J]. *X-ray Spectrometry*, 2005, 34:493-497.
- [33] BJEOUNIKHOV A, GÜNTHER A, RABE J. Realisation of XRD in SEM[C]. *Poster 5, Third German National Conference "Prozessnahe Röntgenanalytik" (X-ray Analytics in Technological Processes)*, 2005.
- [34] BJEOUNIKHOV A, LANGHOFF N, SCHMALZ J, *et al.*. Kompakter mobiler Messkopf für die Element- und Molekülspektrometrie durch die Nutzung der Methodenkopplung (RF- und Raman-Spektroskopie) (Compact mobile measuring Head for Elemental and Molecular Spectroscopy by using Method Coupling (XRF and Raman Spectroscopy)). 11[D]. *Anwendertreffen Röntgenfluoreszenz- und Funkenemissionsspektrometrie*, 8. - 9. März 2004, *Universität Duisburg-Essen*.

**Authors' biography:** **Reiner Wedell** received his diploma degree in Physics in 1973 from the Humboldt University Berlin and Dr. rer. nat. in 1976 from the Moscow State Lomonosov University. In 1980 he received Dr. sc. nat. (Habilitation) from the Humboldt University Berlin for a thesis in the field of channeling radiation. From 1976 until 1992 he worked at the Department of Physics of the Humboldt University as a researcher in the field of interaction of charged particles with matter. From 1994 until 1999 he was employed by the IFG Institut fuer Geraetebau GmbH and worked in projects at X-ray optics and X-ray analytics. In 1999 he became the managing director of the Institut fuer angewandte Photonik e. V. E-mail: wedell-iap@ifg-adlershof.de

(本栏目编辑 李树军)